The LbcA lipoprotein and CtpA protease assemble an oligomeric complex to control peptidoglycan hydrolases in *Pseudomonas aeruginosa*

Hao-Chi Hsu[1], Michelle Wang[2], Amanda Kovach[1], Andrew J. Darwin[2,*], Huilin Li[1,*]

[1]Department of Structural Biology, Van Andel Institute, Grand Rapids, Michigan
[2]Department of Microbiology, New York University Grossman School of Medicine, New York, New York

[*] Correspondence should be addressed to A.D (andrew.darwin@med.nyu.edu) or H.L. (Huilin.Li@vai.org).

ABSTRACT

Pseudomonas aeruginosa CtpA is a carboxyl terminal–processing protease that partners with the outer membrane lipoprotein LbcA to degrade cell wall cross-link hydrolases. This activity plays an important role in supporting *P. aeruginosa* virulence. However, almost nothing is known about the molecular mechanisms underlying CtpA and LbcA function. Here, we used structural analysis to show that CtpA alone assembles into an inactive hexamer comprising a trimer of dimers, which limits its substrate access and prevents nonspecific degradation. The adaptor protein LbcA is a right-handed open spiral with 11 tetratricopeptide repeats, which might wrap around a substrate to deliver it to CtpA for degradation. We found that up to three LbcA molecules can bind to one CtpA hexamer to assemble a giant, active protease complex that degrades its peptidoglycan hydrolase substrates both *in vitro* and *in vivo*. This work reveals an intricate protease activation mechanism that is substrate delivery-dependent and enables targeted removal of the peptidoglycan hydrolase substrates.

INTRODUCTION

A eubacterial cell is protected by a mesh-like cell wall of peptidoglycan (PG; also termed murein), which is composed of linear glycan strands with peptide side chains that cross-link to each other through peptide bonds [1]. To accommodate growth, these cross-links must be cleaved so that nascent PGs can be inserted into the network [1-3]. Several PG endopeptidases carry out this hydrolysis, including MepS, MepM, and MepH in *Escherichia coli* [4,5]. However, if not tightly regulated, their activity could lead to rupture of the PG sacculus and cell death. One way to regulate endopeptidase activity is through the relatively recently discovered carboxyl-terminal processing (CTP) protease system. CTPs belong to the S41 family of serine proteases and include three subfamilies: CTP-1 such as Prc, CTP-2 such as CtpB, and the CTP-3 subfamily CtpA [6]. All CTPs have a PDZ domain — named after the first three proteins the domain was noted in: postsynaptic density protein of 95 kDa, disc large tumor suppressor, and zonula occludens-1 protein — which plays roles in substrate recognition and protease regulation [7,8]. CTPs work within the cell envelope of both Gram-negative and Gram-positive bacteria and have been linked to virulence [9-13].

The *E. coli* CTP-1 protease Prc was found to partner with the lipoprotein adaptor NlpI to cleave the PG endopeptidase MepS [5]. Prc is a bowl-shaped monomeric structure, and the *E. coli* NlpI adaptor contains four tetratricopeptide repeats [14]. NlpI forms a homodimer that binds to two separate molecules of the Prc protease. In *Bacillus subtilis*, the CTP-2 protease CtpB processes and activates the intramembrane protease 4FA-4FB complex, thereby regulating spore formation [15,16]. The *B. subtilis* CtpB has N-terminal and C-terminal dimerization domains, plus a cap domain preceding the protease core domain. Structural analysis revealed that CtpB assembles a dimeric self-compartmentalizing ring structure [17]. The substrate peptide enters the proteolytic site via a narrow tunnel that is largely sequestered by the PDZ domain and becomes exposed only in the presence of a substrate. Therefore, the CtpB protease is reversibly activated by the substrate C-terminal peptide. No structural studies have been reported so far for a CTP-3 protease, which is the topic of the current study.

Pseudomonas aeruginosa is an opportunistic human pathogen. It is one of the leading causes of sepsis in intensive care units, and outbreaks of multidrug-resistant strains have also been reported in hospitals [18-20]. In contrast to *E. coli*, in which the only CTP present is Prc, *P. aeruginosa* has both the CTP-1 protease Prc, and the CTP-3 protease CtpA [10,21]. We reported previously that CtpA is required for normal function of the type 3 secretion system and for

virulence in a mouse model of acute pneumonia [10]. *P. aeruginosa* CtpA shares a 39% amino acid sequence identity with the *B. subtilis* CtpB, which suggests that they might share a similar fold. However, CtpA has a much longer C-terminal region. This extended C-terminus might alter the oligomerization mode relative to that of CtpB [17].We do not know whether or how CtpA assembles into a self-compartmentalizing structure to prevent nonspecific proteolysis. Unlike CtpB, CtpA is not directly activated by a protein substrate. Instead, it requires the adaptor protein LbcA, the lipoprotein binding partner of CtpA, for activity *in vivo* and *in vitro* [22].

LbcA is predicted to be anchored to the outer membrane via acyl chains attached to a Cys residue at the N-terminus of the mature protein, and to contain 11 tetratricopeptide repeats (TPRs). The TPR motif is a degenerate 34-amino-acid sequence that mediates protein–protein interactions [23-25]. LbcA is not a substrate of CtpA; instead, it promotes CtpA protease activity [22]. Therefore, *ctpA* and *lbcA* null mutants share common phenotypes, such as a defective type 3 secretion system and accelerated surface attachment [10,22]. Four LbcA–CtpA substrates have been reported to date, which are all predicted to be PG cross-link hydrolases: the LytM/M23 family peptidases MepM and PA4404, and the NlpC/P60 family peptidases PA1198 and PA1199 [22]. Therefore, it appears that LbcA interacts with CtpA to assemble an active proteolytic complex, which controls the activity of these enzymes by degrading them, but the molecular mechanisms underlying CtpA and LbcA function are unknown. In this manuscript, we describe the crystal structures of CtpA and LbcA, determined separately. We show that CtpA alone assembles as an inactive trimer of dimers. We also report 8-Å-resolution cryo-EM maps of the *in vitro* assembled and active LbcA–CtpA complex. We show that up to three LbcA molecules can bind to the three vertexes of the triangular CtpA complex, and that LbcA activates CtpA by binding to its N-terminal dimerization and cap regions.

RESULTS

1. CtpA assembles a trimer-of-dimers hexamer in solution

CtpA is located in the periplasm, tethered to the outer membrane via its interaction with LbcA [22]. Its N-terminal 23 residues are a type I signal sequence, which is followed by a 14-residue region that is enriched in alanine, glycine, and proline that contributes to a bacterial low complexity region [26] and is predicted to be disordered. We therefore removed these 37 amino acids to produce a truncated CtpA protein for structural and functional studies (**Supplemental Table 1, Fig. 1a**). For simplicity, we refer to this ΔN37 construct as CtpA throughout the main text. The CtpA crystals diffracted X-rays to 3.5-Å resolution. We first used molecular replacement with the

98 *B. subtilis* CtpB as a search model to solve the CtpA structure, but this did not lead to a
99 satisfactory solution. We then produced selenomethionine-substituted CtpA crystals for SAD-
100 based phasing. The derivatized crystals diffracted to 3.3 Å, leading to successful structural
101 solution (**Supplemental Table 2**). CtpA formed a hexamer that comprised a trimer of dimers
102 (**Fig. 1b**). This oligomer state is consistent with an estimated mass of a hexamer from the gel
103 filtration profile (**Fig. 1c**). As expected, each CtpA protomer consists of an N-terminal
104 dimerization region (NDR), a PDZ domain, a cap domain, a protease core domain, and a C-
105 terminal dimerization region (CDR) (**Fig. 1d**). The PDZ domain is partially disordered, but we
106 were able to generate a homolog PDZ model based on the CtpB structure and accurately
107 docked the domain guided by two anomalous density peaks from selenomethionine residues
108 153 and 160 of the domain (**Supplemental Figure 1**). The loop connecting S10 and H6 (aa's
109 378–411) within the CDR was disordered, and the last two residues (435-436) were not
110 resolved.
111
112 **2. The CtpA hexamer alone in the absence of LbcA is in an inactive configuration**
113 The CtpA core region contains the protease active site. There is a narrow tunnel dividing the
114 core domain into the upper cap and lower body regions (**Fig. 1d**); in CtpB this tunnel was
115 suggested to guide the substrate peptide into the proteolytic site [17]. The cap of CtpA is a four-
116 stranded β-sheet (S4, S5, S8, S9) located below the NDR. The body region is composed of a
117 three-helix bundle (H3, H4, H5) and a five-stranded β-sheet (S1, S2, S3, S6, S7). The CtpA
118 catalytic Ser-302 is located at the end of the narrow tunnel between the cap and the body
119 region.
120
121 The CtpA hexamer is in an inactive conformation. The PDZ domain is in a position that blocks
122 the narrow substrate peptide tunnel leading to Ser-302. Furthermore, the catalytic triad Ser-
123 302–Lys-327–Gln-331 is well beyond hydrogen-bonding distance: Ser-302 and Lys-327 are 4.2
124 Å apart and Lys-327 and Gln-331 are 8 Å apart (**Fig. 1e**). We solved the crystal structure of
125 CtpA that was catalytically inactive due to an S302A substitution and found that it was also in
126 the inactive configuration (**Supplemental Figure 2**). For comparison, the catalytic triad Ser-
127 309–Lys-334–Gln-338 in the protease-active *B. subtilis* CtpB are all within hydrogen-bonding
128 distance (**Fig. 1e**). By superimposing the two proteases, we found that transition to the active
129 form requires the CtpA cap domain to clamp down toward the catalytic site by 11 Å and also a
130 large-scale movement of the associated PDZ domain by 12 Å (**Fig. 1f, Supplemental Video 1**).
131 The CtpA structure is consistent with our previous observation that purified wild-type CtpA alone

132 was inactive in degrading its substrates [22]. The addition of purified LbcA was able to activate the
133 protease of wild-type CtpA but not of the mutant CtpA(S302A). Therefore, unlike CtpB, which
134 fluctuates between an active and inactive form in solution and can be activated by a protein
135 substrate [17], the CtpA hexamer is locked in an inactive configuration and requires LbcA for
136 activation [22].
137
138 **3. The N- and C-terminal dimerization interfaces are important for full CtpA activity**
139 *P. aeruginosa* CtpA dimerizes via its NDR in the same way as *B. subtilis* CtpB (**Fig. 2a**).
140 However, the two CDRs of CtpA are far apart in this dimer, and six unhinged CDRs of three
141 CtpA dimers interact to form the triangular trimer-of-dimer complex (**Figs. 1b, 2a**). In contrast,
142 CtpB forms a parallel homodimer by both head-to-head N-terminal and tail-to-tail C-terminal
143 interactions (**Fig. 2b**) [17]. The CtpA NDR is composed of the H1 and H2 helices. The NDRs of
144 two CtpA monomers form a domain-swapped, intermolecular 4-helix bundle, in which the NDR
145 of one protomer reaches over to contact the cap domain of the other protomer (**Fig. 2a, 2c**). The
146 four-helix bundle is at the vertex of the triangular complex. The NDR–NDR dimerization is driven
147 by hydrophobic interactions. Specifically, Leu-69, Ala-73, and Met-77 are at the intersecting
148 point of the two crossed H2's. Met-77 hydrophobically interacts with Leu-53 and Leu-69 of the
149 second protomer (**Fig. 2c**). H1 of protomer 1 is nearly parallel to H2 of protomer 2, with the H1
150 residues Leu-46, Phe-49, Val-52, Leu-53, and Val-56 hydrophobically interacting with the H2
151 residues Leu-70, Ile-74, Met-77, Leu-78, and Leu-81. The Leu-46 and Phe-49 of the two H1's
152 are also within the van der Waals distance. The hydrophobic NDR–NDR interaction of the CtpA
153 dimer resembles that in the CptB dimer, consistent with the conserved sequence in this region
154 (**Fig. 2e**). As described below, the CtpA NDR is the primary binding site of LbcA, indicating the
155 importance of the region for function.
156
157 The C-terminal dimerization interface of CtpA involves the β-strand S10 and the helix H6 (**Fig.**
158 **2d**). The two S10 β-strands (Arg-370 to Glu-376) form an intermolecular, antiparallel β-sheet
159 that reinforces the dimer interface. The two H6's (Tyr-418 to Gly-435) are orthogonal to each
160 other but form a short leucine zipper in the middle section mediated by Leu-426 and Leu-430.
161 The CtpA C-terminal dimer interface is not like that of CtpB, which dimerizes via interaction in a
162 different region. Indeed, the C-terminal sequence of *P. aeruginosa* CtpA is not conserved in *B.*
163 *subtilis* CtpB (**Fig. 2e**), which is consistent with their different oligomeric assembly. To
164 investigate the functional importance of the unique C-terminal dimerization interface of CtpA, we
165 constructed a mutant with a partially disrupted H6 helix by removing the last six residues (Ser-

166 431 to Asn-436; CtpA(ΔC6); **Fig. 1a**). We found that CtpA(ΔC6) eluted from a gel filtration
167 column as a dimer (**Fig. 1b**), so the C-terminal truncation prevented CtpA hexamer formation.
168 Cryo-EM 2D class averages and 3D reconstruction confirmed that this mutant protein
169 assembled as a dimer, not a hexamer (**Fig. 2f-g**), and the two subunits expanded outward by 4
170 Å relative to the CtpA dimer in the hexamer (**Fig. 2g**).
171
172 We next asked whether the C-terminal dimerization interface, present in the intact CtpA
173 hexamer but disrupted in the CtpA(ΔC6) dimer, is required for LbcA binding and LbcA-mediated
174 activation of CtpA. We co-expressed CtpA(ΔC6) and LbcA and found that only a small amount
175 of LbcA bound to the dimer (**Fig. 3a**). As described below, LbcA binds to the full-length CtpA at
176 much higher stoichiometry. In an *in vitro* assay, we found that LbcA was less active with the
177 CtpA(ΔC6) dimer than with the CtpA hexamer in degrading the model substrate PA1198
178 (compare lanes 3 and 4 in **Fig. 3c**).
179
180 To further investigate the functional significance of the leucine zipper in H6, we generated two
181 CtpA double-mutant constructs with L426K/L430K and L426A/L430A substitutions that
182 disrupted the leucine zipper interaction. The two purified mutant proteins were mainly dimeric
183 and failed to assemble into a hexamer, based on their gel filtration profiles (**Fig. 3b**). Their
184 LbcA-activated *in vitro* protease activity toward PA1198 was lower relative to wild-type CtpA
185 (**Fig. 3c**, compare lanes 5 and 6 to lane 3). However, like the CtpA(ΔC6) mutant, the leucine
186 zipper mutants retained significant protease activity relative to the protease dead mutant
187 CtpA(S302A) (**Fig. 3c**, compare lanes 5 and 6 with lane 2).
188
189 We extended our analysis by constructing plasmids encoding derivatives of full-length CtpA with
190 the ΔC6, L426K/L430K (LLKK), or L426A/L430A (LLAA) mutations. After introducing these
191 plasmids into a *P. aeruginosa* Δ*ctpA* mutant, immunoblot analysis showed that the steady-state
192 levels of the mutant proteins were the same as those of the wild type (**Fig. 3d**). Therefore, the
193 mutations did not affect CtpA stability *in vivo*. However, PA1198 accumulated in the presence of
194 these three mutants relative to the wild type, although not as much as in the presence of
195 CtpA(S302A) (**Fig. 3d**). This suggests that the protease activity of the three mutants was
196 reduced, but not abolished, which is consistent with the *in vitro* analysis. Therefore, our studies
197 suggest that the hexameric assembly is important for proper CtpA function.
198
199 **4. LbcA forms a spiral that could wrap around CtpA substrates**

200 During the maturation of the lipoprotein LbcA, its N-terminal 16 residues are removed, exposing
201 Cys-17 (**Fig. 4a**). Then Cys-17 is lipidated so that the N-terminus can be anchored in the outer
202 membrane from the periplasmic side [27-29]. LbcA is able to bind to CtpA and its substrates
203 independently (D. Chakraborty and A. J. Darwin, manuscript submitted). Therefore, in order to
204 understand how LbcA recruits the substrates and activates CtpA, we tried to solve the LbcA
205 crystal structure. We were able to crystallize LbcA with its N-terminal 47 residues removed
206 (ΔN47). The crystal structure was solved to 3.5-Å resolution by the SAD method with
207 selenomethionine-derivatized LbcA(ΔN47) crystals (**Fig. 4a-d**). This structure contains only α-
208 helices and connecting loops, with a total of 29 α-helices. We resolved all 11 predicted
209 tetratricopeptide repeats, comprising 22 α-helices from helix-7 (H7) to H28. The sequences of
210 the 34-residue TPRs are largely conserved (**Fig. 4b**). Gly/Ala at position 8 and Ala at positions
211 20 and 27 are most conserved in the TPR family, although none of these are invariant.
212 Interestingly, TPR1, TPR5, and TPR10 contain only 33 amino acids, but they all contain the
213 signature residues Gly/Ala at position 8 and Ala at position 20. TPR1 and TPR10 contain an
214 additional signature Leu at position 24. Within each TPR, the first helix (TPR-A) lines the outer
215 surface and the second helix (TPR-B) lines the inner surface of the ring structure. Alignment of
216 the 11 TPRs in LbcA(ΔN47) showed that more-conserved hydrophobic residues are
217 concentrated in the TPR-A helix and more-conserved charged residues are distributed in TPR-B
218 helix and in the turns connecting TPR-A and TPR-B, suggesting that the inner and the outer
219 surfaces of the ring may have distinct functions.
220
221 The 11 TPRs form a notched ring, with an outer diameter of about 6 nm and an inner diameter
222 of about 3 nm (**Fig. 4c**). Because the first TPR is slightly above, and the last TPR is below the
223 ring, it is a right-handed spiral structure. The first 4 α-helices at the N terminus form an
224 elongated extension that partially caps the TPR ring. Helices H5 and H6 serve as a hinge that
225 links the N-terminal helical extension and the TPR spiral. However, the loop connecting H4 and
226 H5 (aa's 163-171) has a high crystallographic B-factor that is indicative of flexibility. Therefore,
227 this loop and the H5-H6 hinge are likely to allow relative motion of the NT helical extension with
228 respect to the TPR spiral. The TPR ring is capped at the end by the single short α-helix, H29.
229
230 Four LbcA(ΔN47) molecules formed an interlocked tetramer as a dimer of dimers in the crystal,
231 although the truncated LbcA purified as a monomer in solution (**Supplementary Figure 3**). The
232 chamber of the TPR spiral of the first LbcA is occupied by the H3-H4 of a second LbcA

233 molecule on the top and by the H1-H2 of a third LbcA molecule on the side (**Fig. 4d**). Therefore,
234 there is a 4-helix bundle inside the first LbcA TPR spiral. We suggest that this bundle may mimic
235 a substrate and that the LbcA spiral may wrap around the PG hydrolase substrate to target it to
236 CtpA for degradation. In this scenario, the conserved and charged residues of the TPR-B
237 helices lining the inner surface of the TPR spiral may participate in binding that substrate.
238
239 **5. LbcA and CtpA assemble a giant 3:6 active protease complex**
240 To study how LbcA interacts with CtpA to assemble an active protease complex, we co-
241 expressed the LbcA–CtpA complex using the protease-dead mutant CtpA(S302A). To enhance
242 LbcA binding to CtpA, we made a new LbcA construct (ΔN31) that included 16 more residues at
243 the N-terminus than LbcA(ΔN47). The binding between LbcA and CtpA was strong enough to
244 survive gel filtration chromatography. SDS-PAGE analysis of the purified protein complex
245 suggested a molar ratio of 1:2 between LbcA and CtpA (**Fig. 5a**), suggesting that three LbcA
246 molecules can bind to a single trimer-of-dimer CtpA hexamer, forming a giant, 420-kDa, 3:6
247 protease complex. However, we were unable to crystallize this complex, probably due to its
248 flexibility. Therefore, we next tried cryo-EM analysis.
249
250 **6. Cryo-EM reveals two major conformations of the CtpA–LbcA complex**
251 The 3:6 LbcA(ΔN31)–CtpA complex was purified by gel filtration chromatography in a mild buffer
252 containing 10 mM Tris, pH 8.0, and 150 mM NaCl. The 2D class averages of the cryo-EM
253 particle images confirmed the assembly of the 3:6 complex, with one LbcA(ΔN31) bound on
254 each of the three vertexes of the CtpA trimer and dimers (**Fig. 5b**). The LbcA appeared to
255 associate flexibly with CtpA, leading to the LbcA density being largely averaged out in many 2D
256 class images, and only a partial (and often a single) LbcA molecule was clearly visible.
257 Therefore, we focused on classification and 3D reconstruction on a single vertex and obtained
258 two cryo-EM 3D maps at 8-Å average resolution (**Supplemental Figure 4**). The resolution could
259 not be improved due to the flexible association as well as the flexibility of the LbcA spiral itself.
260
261 The two cryo-EM maps probably represent two functional conformations of LbcA bound to the
262 CtpA hexamer (**Fig. 5c, Supplemental Video 2**). In conformer I, LbcA only has one contact at
263 the top of the CtpA hexamer, which is likely to involve the N-terminal helical extension of LbcA
264 with the top two H1 helices of the CtpA dimer. In conformer II, the LbcA spiral moves down
265 toward CtpA by as much as 20 Å. The spiral region of the LbcA(ΔN47) crystal structure fits the
266 cryo-EM density nicely, with the N-terminus of the spiral approaching CtpA. The crystal structure

267 of the LbcA(ΔN47) NT helical extension didn't fit in the density, and this region was therefore
268 removed from docking. This observation is consistent with the LbcA(ΔN47) crystal structure in
269 which the H5-H6 hinge region connecting the NT helical extension and the spiral is flexible,
270 such that the helical extension when bound to CtpA has taken on a different configuration than
271 in the crystal structure.
272
273 The hexameric CtpA crystal structure fitted well with the cryo-EM map, except for the PDZ
274 domains (**Fig. 5d**). Upon LbcA binding, the front PDZ domain of the top CtpA dimer rotates and
275 moves outwards by 9 Å, away from the hexameric plane, enlarging the substrate peptide
276 binding pocket. A similar PDZ domain movement was also observed in the CtpB structure and
277 was associated with the conversion from an inactive to an active protease [17].
278
279 **7. The LbcA H1 is essential for binding to and activating the CtpA protease**
280 Docking of the right-handed LbcA spiral crystal structure into the cryo-EM map points the LbcA
281 N-terminus toward the NDRs of the top CtpA dimer. This suggests that initial engagement
282 between LbcA and CtpA involves the LbcA N-terminal helical extension and the CtpA NDR. To
283 test this hypothesis, and to identify the binding interface more accurately, we produced a series
284 of N- and/or C-terminal-truncated LbcA mutants and did a CtpA pulldown assay (**Fig. 6a**). We
285 found that removing the C-terminal five residues of LbcA did not affect the LbcA–CtpA
286 interaction, consistent with the docking result in which the LbcA N-terminal region (not the C-
287 terminal region) interacts with CtpA. All constructs containing the complete H1-H29 region
288 pulled down CtpA. However, LbcA with either H1 truncation (His_6-LbcAΔN84) or H1-H4
289 truncation (His_6-LbcAΔN165) failed to pull down CtpA. This result suggests that the LbcA NT
290 helical extension, in particular H1, is required for LbcA binding to CtpA, and that LbcA H1
291 directly participates in the binding.
292
293 We then carried out both *in vitro* and *in vivo* assays to monitor degradation of the PA1198
294 substrate [22]. We first incubated purified CtpA with separately purified LbcA proteins and purified
295 PA1198. As expected, PA1198 was degraded in the presence of His_6-LbcAΔN47, which had the
296 intact NT helical extension (**Fig. 6b**). However, PA1198 was not degraded in the presence of
297 His_6-LbcA(ΔN84) (missing H1) or His_6-LbcA(ΔN165) (missing H1-H4). In fact, the outcomes of
298 reactions with these two truncations were indistinguishable from those containing no LbcA or
299 those using the protease dead CtpA(S302) (**Fig. 6b**). In a Δ*lbcA* mutant *P. aeruginosa* strain,

300 plasmids encoding LbcA with in-frame truncations equivalent to the ΔN84 or ΔN165 constructs
301 failed to activate CtpA, as revealed by the accumulation of PA1198, which was present at a
302 similar level as in a strain without any LbcA (**Fig. 6c**). Therefore, both pulldown and *in vitro* and
303 *in vivo* activity assays pinpointed the LbcA H1 as a key binding element for activation of the
304 CtpA protease.
305
306 **DISCUSSION**
307 The LbcA–CtpA system supports the function of the *P. aeruginosa* type 3 secretion system; is
308 required for virulence in a mouse model of acute infection; and affects surface attachment [10,22].
309 Furthermore, four CtpA substrates are PG cross-link hydrolases, which means that the LbcA–
310 CtpA system affects the integrity of a crucial cell envelope component and perhaps the most
311 important antibiotic target, the cell wall. Therefore, this system itself could be an effective
312 antibiotic target, and the structural analysis reported here may aid the development of such
313 antibiotics. We have shown that CtpA assembles as a hexamer. However, the hexamer alone is
314 inactive, because the catalytic triad Ser302–Lys327–Gln331 is not in hydrogen-bonding
315 distance. We found that the CtpA partner protein LbcA is a spiral with a large cavity that has the
316 capacity to wrap around a substrate. Together, LbcA and CtpA assemble a giant complex with a
317 stoichiometry of up to 3:6. Our cryo-EM experiments captured two conformations of this
318 complex that differ in the position of the LbcA spiral. In conformer I, LbcA H1 primarily interacts
319 with the two H1 helices of a CtpA dimer. Transiting to conformer II, the TPR spiral descends and
320 makes a second contact with the cap region of CtpA, leading to an outward movement of the
321 PDZ domain. These concerted changes are likely to underlie the activation of the CtpA
322 protease.
323
324 Based on the structures and the activity assays, we propose the following CtpA activation
325 mechanism (**Fig. 7**). In the absence of its partner, CtpA is in an inactive hexamer form. When a
326 substrate-bound LbcA encounters CtpA, the N-terminal extension of LbcA first engages the
327 CtpA N-terminal dimerization domain. The initial LbcA engagement likely triggers changes in
328 both CtpA and LbcA. The CtpA PDZ domain moves 9 Å away from the catalytic site, creating a
329 substrate peptide-binding pocket, and the main body of the LbcA superhelix moves towards
330 CtpA by 20 Å to interact with the CtpA cap region, likely triggering a rearrangement of the
331 catalytic triad into the active configuration. Accompanying the large LbcA movement, the C-
332 terminal peptide of the LbcA-bound substrate inserts into the newly formed and just-activated
333 CtpA catalytic site for degradation. This is an on-demand, reversible activation mechanism. The

334 CtpA protease activity is controlled by the presence of a substrate bound LbcA partner, and its
335 CtpA activation is reversible because degradation of the substrate will lead to the dissociation of
336 LbcA, and the CtpA hexamer will revert to its inactive configuration.
337
338 However, it is equally possible that LbcA and CtpA are always in complex. This alternative is
339 supported by our previous experiments suggesting that most, if not all, CtpA in the cell is bound
340 to LbcA [22]. CtpA fractionates with the membrane fraction in *lbcA*$^+$ cells but is in the soluble
341 periplasm in Δ*lbcA* cells, and when CtpA or LbcA are purified from *P. aeruginosa*, they bring a
342 lot of the other one down with them [22]. Also, the pulldown assays done here show that LbcA and
343 CtpA can interact in the absence of substrate (**Fig. 6a**). In this scenario, the LbcA-CtpA
344 fluctuates between inactive and active states (conformers I and II), and perhaps the presence of
345 a substrate would stabilize the enzyme-adaptor-substrate in the active state for productive
346 substrate hydrolase degradation.
347
348 Both the elution volume in the gel filtration profile and the cryo-EM 2D class averages indicate
349 that LbcA and CtpA assemble a 3:6 stoichiometric complex that has one molecule of LbcA
350 bound to each of the three vertexes of the CtpA trimer-of-dimers. Because LbcA is anchored to
351 the outer membrane *in vivo*, the CtpA hexamer in the full complex (3:6) is held nearly parallel to
352 the membrane by three LbcA, i.e., with the 3-fold symmetry axis perpendicular to the membrane
353 plane. However, a strict 3:6 stoichiometry may not be necessary and that CtpA can be activated
354 when one LbcA molecule binds a substrate hydrolase.
355
356 The PDZ domain is the C-terminal peptide substrate-binding element of the CTPs [30]. The ability
357 of PDZ domains to move in order to accommodate the incoming C-terminal substrate peptide
358 partially accounts for the substrate delivery–based activation mechanism of the CTPs. The PDZ
359 domain is the most flexible region in the CtpB structure. The PDZ there acts as an inhibitor by
360 blocking the substrate peptide binding in the inactive form, but it moves away to form a narrow
361 tunnel for a substrate peptide in the active form [17]. Similarly, the PDZ domain of CtpA is highly
362 flexible and largely invisible in the crystal structure of inactive CtpA hexamer. This domain
363 moves away from the active site in the active, LbcA-bound CtpA complex, perhaps suggesting a
364 activation mechanism similar to that of CtpB. In the case of CTP-1 family member Prc from *E.*
365 *coli*, the PDZ domain acts as an activator rather than an inhibitor, but its movement is still a key
366 feature of the activation mechanism [8]. Therefore, our work on a CTP-3 family member
367 underscores nature's general design principle for the CTPs by combining a classic serine

368 protease module with a C-terminal binding domain to generate a diverse set of enzymes for
369 regulated proteolysis [30].
370
371 A feature of *P. aeruginosa* CtpA is the requirement of the partner lipoprotein LbcA for activation
372 and targeted proteolysis [22]. This is a variation in the general substrate activation mechanism. In
373 this regard, the LbcA–CtpA system is analogous to the *E. coli* NlpI–Prc system, in which the
374 TPR-containing adaptor NlpI plays the dual function of delivering the PG hydrolase MepS to the
375 Prc protease for degradation and activating the protease [8,14]. Despite this functional similarity,
376 significant differences exist between these two systems. The two proteases are in different CTP
377 subfamilies; *E. coli* Prc is much larger than *P. aeruginosa* CtpA; and Prc functions as a
378 monomer, not a hexamer. Therefore, the Prc N-terminal and C-terminal helical domains are not
379 involved in oligomerization; instead, they wrap around the protease core, perhaps to limit
380 substrate access to the protease. NlpI has a total of 14 helices with four TPRs, compared with
381 the 29 helices and 11 TPRs of LbcA. Although NlpI and LbcA both contain TPRs, the primary
382 sequences of the proteins are not similar. Finally, NlpI functions as a dimer, unlike the
383 monomeric state of LbcA.
384
385 The LbcA–CtpA system contributes to the virulence of *P. aeruginosa*. This makes
386 understanding the structure and function of this proteolytic system broadly significant. A future
387 challenge is to understand how the different substrates, not just peptides, are specifically
388 recognized by the multitude of CTPs and/or their adaptor proteins for tightly regulated
389 proteolysis.
390
391 **Acknowledgements.** Diffraction data for CtpA were collected at the Lilly Research Laboratories
392 Collaborative Access Team (LRL-CAT) beamline and diffraction data of LbcA were collected at
393 the Life Sciences Collaborative Access Team (LS-CAT) beamline of the Advanced Photon Source
394 (APS). The APS is a U.S. Department of Energy (DOE) Office of Science User Facility operated for
395 the DOE Office of Science by Argonne National Laboratory under Contract No. DE-AC02-
396 06CH11357. Cryo-EM data were collected at the David Van Andel Advanced Cryo-Electron
397 Microscopy Suite at Van Andel Institute. We thank Dolonchapa Chakraborty for supplying
398 plasmid pAJD2948 and His_6-PA1198 protein, Gongpu Zhao and Xing Meng for help with data
399 collection, and David Nadziejka for technical editing of the manuscript. This study was

supported by U.S. National Institutes of Health grant R01 AI136901 (to A.D.) and by Van Andel Institute (to H.L.).

Author contributions. H.H., A.D., and H.L. conceived and designed experiments. H.H., M.W., A.K. performed biochemical and microbiological experiments. H.H. performed protein crystallography and cryo-EM. H.H., A.D., and H.L. analyzed the data and wrote the manuscript with input from all authors.

Data Availability. The crystal structures of CtpA and LbcA have been deposited in the Protein Data Bank under accession codes xxx1 and xxx2. Cryo-EM 3D maps of the CtpA–LbcA complex in conformations I and II at approximately 10-Å resolution have been deposited in the Electron Microscopy Data Bank under accession codes EMD-yyy1 and EMD-yyy2.

REFERENCES

1. Vollmer, W., Blanot, D. & de Pedro, M.A. Peptidoglycan structure and architecture. *FEMS Microbiol Rev* **32**, 149-67 (2008).
2. Pazos, M., Peters, K. & Vollmer, W. Robust peptidoglycan growth by dynamic and variable multi-protein complexes. *Curr Opin Microbiol* **36**, 55-61 (2017).
3. Vollmer, W. Bacterial growth does require peptidoglycan hydrolases. *Mol Microbiol* **86**, 1031-5 (2012).
4. Park, S.H., Kim, Y.J., Lee, H.B., Seok, Y.J. & Lee, C.R. Genetic Evidence for Distinct Functions of Peptidoglycan Endopeptidases in Escherichia coli. *Front Microbiol* **11**, 565767 (2020).
5. Singh, S.K., Parveen, S., SaiSree, L. & Reddy, M. Regulated proteolysis of a cross-link-specific peptidoglycan hydrolase contributes to bacterial morphogenesis. *Proc Natl Acad Sci U S A* **112**, 10956-61 (2015).
6. Rawlings, N.D., Barrett, A.J. & Bateman, A. MEROPS: the peptidase database. *Nucleic Acids Res* **38**, D227-33 (2010).
7. Ye, F. & Zhang, M. Structures and target recognition modes of PDZ domains: recurring themes and emerging pictures. *Biochem. J.* **455**, 1-14 (2013).
8. Chueh, C.K. et al. Structural Basis for the Differential Regulatory Roles of the PDZ Domain in C-Terminal Processing Proteases. *mBio* **10**(2019).
9. Bandara, A.B., Sriranganathan, N., Schurig, G.G. & Boyle, S.M. Carboxyl-terminal protease regulates Brucella suis morphology in culture and persistence in macrophages and mice. *J Bacteriol* **187**, 5767-75 (2005).
10. Seo, J. & Darwin, A.J. The Pseudomonas aeruginosa periplasmic protease CtpA can affect systems that impact its ability to mount both acute and chronic infections. *Infect Immun* **81**, 4561-70 (2013).
11. Deng, C.Y. et al. The periplasmic PDZ domain-containing protein Prc modulates full virulence, envelops stress responses, and directly interacts with dipeptidyl peptidase of Xanthomonas oryzae pv. oryzae. *Mol Plant Microbe Interact* **27**, 101-12 (2014).
12. Carroll, R.K. et al. The lone S41 family C-terminal processing protease in Staphylococcus aureus is localized to the cell wall and contributes to virulence. *Microbiology (Reading)* **160**, 1737-1748 (2014).

13. Bandara, A.B. et al. A disruption of ctpA encoding carboxy-terminal protease attenuates Burkholderia mallei and induces partial protection in CD1 mice. *Microb Pathog* **45**, 207-16 (2008).
14. Su, M.Y. et al. Structural basis of adaptor-mediated protein degradation by the tail-specific PDZ-protease Prc. *Nat Commun* **8**, 1516 (2017).
15. Campo, N. & Rudner, D.Z. A branched pathway governing the activation of a developmental transcription factor by regulated intramembrane proteolysis. *Mol Cell* **23**, 25-35 (2006).
16. Rudner, D.Z. & Losick, R. A sporulation membrane protein tethers the pro-sigmaK processing enzyme to its inhibitor and dictates its subcellular localization. *Genes Dev* **16**, 1007-18 (2002).
17. Mastny, M. et al. CtpB assembles a gated protease tunnel regulating cell-cell signaling during spore formation in Bacillus subtilis. *Cell* **155**, 647-58 (2013).
18. Paterson, D.L. The epidemiological profile of infections with multidrug-resistant Pseudomonas aeruginosa and Acinetobacter species. *Clin Infect Dis* **43 Suppl 2**, S43-8 (2006).
19. Tumbarello, M. et al. Clinical outcomes of Pseudomonas aeruginosa pneumonia in intensive care unit patients. *Intensive Care Med* **39**, 682-92 (2013).
20. Crivaro, V. et al. Pseudomonas aeruginosa in a neonatal intensive care unit: molecular epidemiology and infection control measures. *BMC Infect Dis* **9**, 70 (2009).
21. Hoge, R., Laschinski, M., Jaeger, K.E., Wilhelm, S. & Rosenau, F. The subcellular localization of a C-terminal processing protease in Pseudomonas aeruginosa. *FEMS Microbiol Lett* **316**, 23-30 (2011).
22. Srivastava, D. et al. A Proteolytic Complex Targets Multiple Cell Wall Hydrolases in Pseudomonas aeruginosa. *mBio* **9**(2018).
23. Graham, J.B., Canniff, N.P. & Hebert, D.N. TPR-containing proteins control protein organization and homeostasis for the endoplasmic reticulum. *Crit Rev Biochem Mol Biol* **54**, 103-118 (2019).
24. Zeytuni, N. & Zarivach, R. Structural and functional discussion of the tetra-trico-peptide repeat, a protein interaction module. *Structure* **20**, 397-405 (2012).
25. Blatch, G.L. & Lassle, M. The tetratricopeptide repeat: a structural motif mediating protein-protein interactions. *Bioessays* **21**, 932-9 (1999).
26. Ntountoumi, C. et al. Low complexity regions in the proteins of prokaryotes perform important functional roles and are highly conserved. *Nucleic Acids Res* **47**, 9998-10009 (2019).
27. Konovalova, A. & Silhavy, T.J. Outer membrane lipoprotein biogenesis: Lol is not the end. *Philos Trans R Soc Lond B Biol Sci* **370**(2015).
28. Lewenza, S., Mhlanga, M.M. & Pugsley, A.P. Novel inner membrane retention signals in *Pseudomonas aeruginosa* lipoproteins. *J Bacteriol* **190**, 6119-25 (2008).
29. Narita, S. & Tokuda, H. Amino acids at positions 3 and 4 determine the membrane specificity of *Pseudomonas aeruginosa* lipoproteins. *J Biol Chem* **282**, 13372-8 (2007).
30. Clausen, T., Kaiser, M., Huber, R. & Ehrmann, M. HTRA proteases: regulated proteolysis in protein quality control. *Nat Rev Mol Cell Biol* **12**, 152-62 (2011).
31. Chung, S. & Darwin, A.J. The C-terminus of substrates is critical but not sufficient for their degradation by the Pseudomonas aeruginosa CtpA protease. *J Bacteriol* (2020).
32. Heckman, K.L. & Pease, L.R. Gene splicing and mutagenesis by PCR-driven overlap extension. *Nat. Protoc.* **2**, 924-932 (2007).
33. Choi, K.H., Kumar, A. & Schweizer, H.P. A 10-min method for preparation of highly electrocompetent *Pseudomonas aeruginosa* cells: application for DNA fragment transfer between chromosomes and plasmid transformation. *J. Microbiol. Methods.* **64**, 391-397 (2006).

34. Strom, M.S. & Lory, S. Cloning and expression of the pilin gene of *Pseudomonas aeruginosa* PAK in *Escherichia coli*. *J. Bacteriol.* **165**, 367-372 (1986).
35. Studier, F.W., Rosenberg, A.H., Dunn, J.J. & Dubendorff, J.W. Use of T7 RNA polymerase to direct expression of cloned genes. *Methods in Enzymology* **185**, 60-89 (1990).
36. Qiu, D., Damron, F.H., Mima, T., Schweizer, H.P. & Yu, H.D. PBAD-based shuttle vectors for functional analysis of toxic and highly regulated genes in *Pseudomonas* and *Burkholderia* spp. and other bacteria. *Appl. Environ. Microbiol.* **74**, 7422-7426 (2008).

505 **FIGURES AND LEGENDS**

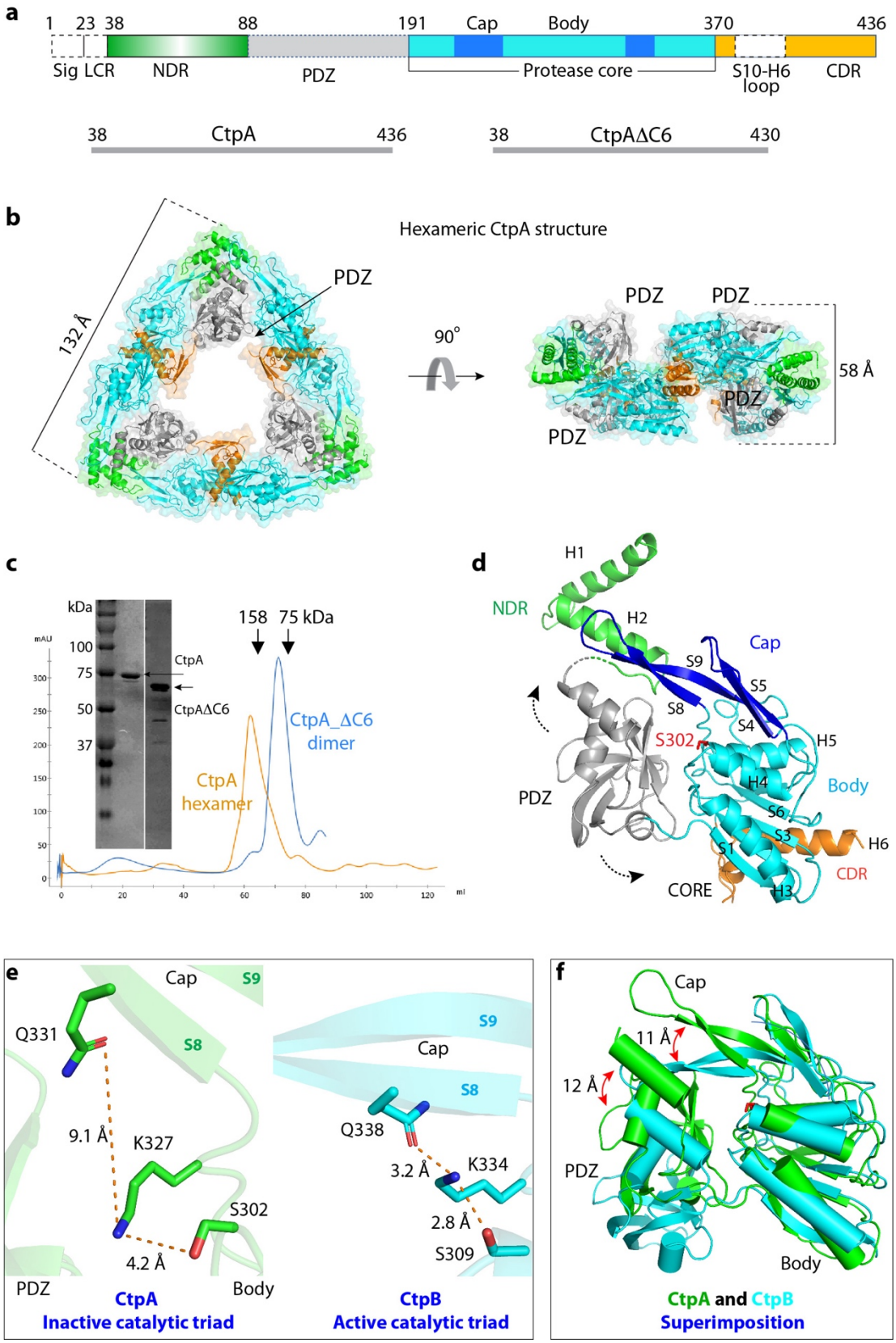

506

507 **Fig. 1**. **Overall structure of CtpA. a**) Top: CtpA domain organization. The dashed lines indicate
508 the disordered regions (PDZ and the S10-H6 connecting loop) that are not resolved in the
509 crystal structure. NDR, N-terminal dimerization region; CDR, C-terminal dimerization region.
510 The sequence ranges of the two CtpA constructs used this study are shown in the lower panels.
511 **b**) Cartoon and transparent surface views of CtpA hexamer. The domains are colored according
512 to the depiction in panel a. **c**) Gel filtration profiles of CtpA and CtpA(ΔC6). Inserted are SDS-
513 PAGE gels of purified CtpA (lane 2) and CtpA(ΔC6) (lane 3). **d**) A CtpA subunit in cartoon view.
514 Secondary structural elements in CtpA are labeled, except in the PDZ domain. The two dashed
515 arrows indicate the mobile PDZ domain in the CtpA hexamer. **e**) Comparison of the catalytic
516 triads of Pa CtpA and Bs CtpB (PDB ID 4C2E). The S8 and S9 labels refer to β-strands 8 and 9
517 in the cap region. **f**) Superposition of the core domains of inactive Pa CtpA (green) and active
518 Bs CtpB (cyan). Catalytic Ser-302 in CtpA and Ser-309 in CtpB are in red sticks. Red arrows
519 indicate lifted-up (CtpA) and clamped-down positions (CtpB) of the cap subdomains.
520

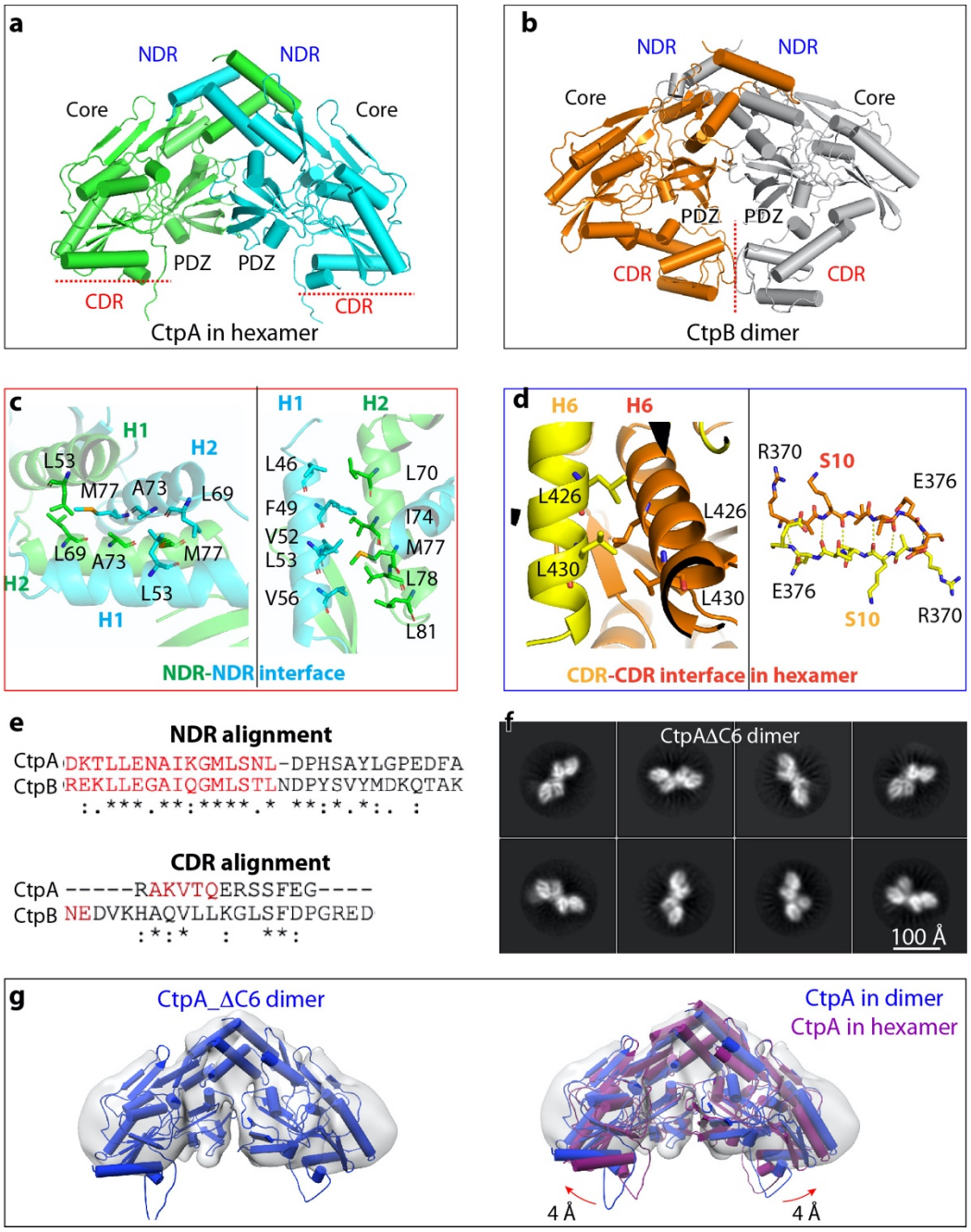

Figure 2. Different oligomerization modes of Pa CtpA and Bs CtpB. **a**) A CtpA dimer extracted from the CtpA hexamer. **b**) Bs CtpB dimer (PDB ID 4C2E). **c**) The N-terminal dimerization interface of CtpA involves hydrophobic interactions between two H2 (left) and between H1 and H2 (right). **d**) The C-terminal dimerization interface of CtpA involves a short leucine zipper-like interaction between two H6 helices and antiparallel β-sheet formation between two S10. **e**) Alignment of the conserved NDR sequence and divergent CDR between Pa CtpA and Bs CtpB. **f)** 2D class averages of the CtpA(ΔC6) dimer. **g**) Left: 3D map of the CtpA(ΔC6) dimer rigid-body-fitted with two CtpA subunits. Right: Superposition of CtpA(ΔC6) dimer model (blue) and the CtpA dimer structure extracted from the hexameric crystal structure (purple).

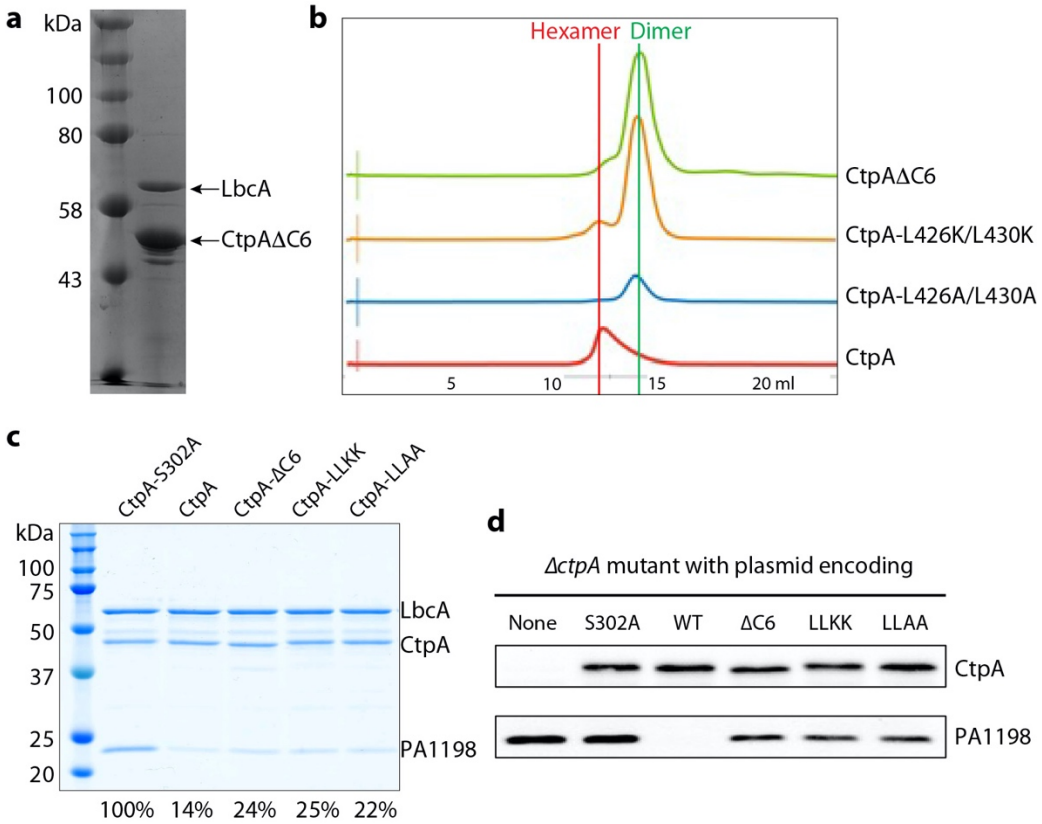

Fig. 3. **Full protease activity of CtpA requires C-terminal dimerization region. a**) SDS-PAGE of gel-filtration peak fraction representing the CtpA(ΔC6)–LbcA complex. LbcA(ΔN47) was used for gel filtration chromatography because this protein could be produced in large quantity at high concentration. **b**) Elution profiles of wild-type and mutant CtpA proteins. **c**) Substrate degradation assay *in vitro*. His_6-PA1198 served as the substrate for the assay. Gels from a single experiment are shown, but the amount of PA1198 degradation is the average from two independent experiments, determined as described in Methods. The number below each lane is the percentage of remaining PA1198 after 3 h, relative to the first lane using the inactive CtpA. **d**) Substrate degradation *in vivo*. Plasmid-encoded protease-dead CtpA(S302A), wild type (WT), ΔC6, L426K/L430K (LLKK), L426A/L430A (LLAA) were produced in a *P. aeruginosa* Δ*ctpA* strain. None = empty plasmid vector control. The CtpA proteins and accumulation of the PA1198 substrate were detected by immunoblot analysis with polyclonal antisera.

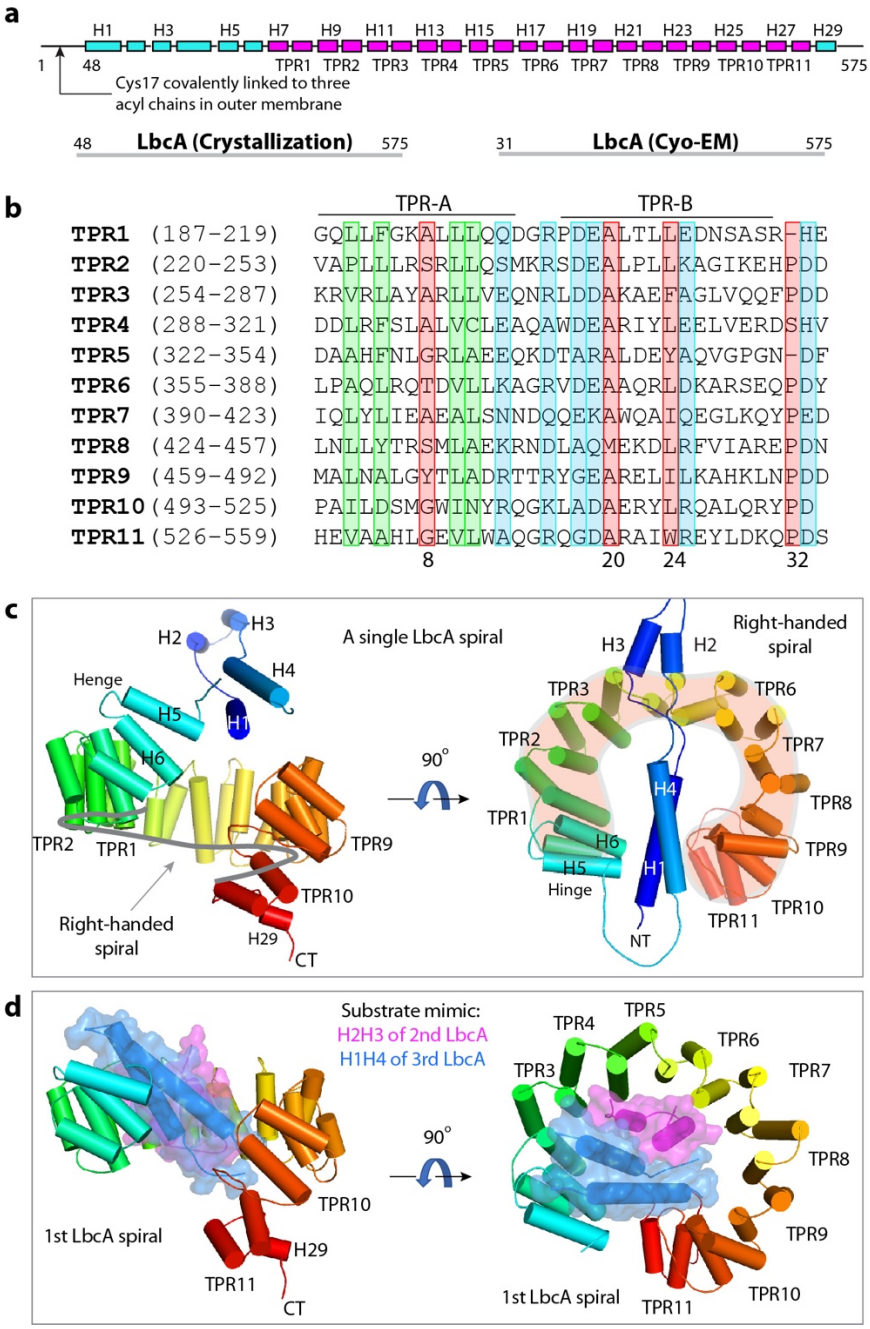

Fig. 4. **Overall structure of LbcA. a**) Domain organization of LbcA. The TPR motifs are shown in magenta. Also shown are two LbcA constructs used in this study. **b**) Sequence alignment of the 11 TPRs of LbcA. The signature residues of TPR are marked in the red rectangles. The highly homologous hydrophobic residues are in green boxes and the highly homologous charged residues are in the blue boxes. **c**) The crystal structure of LbcA(ΔN47) contains an N-terminal extension with 4 helices and a C-terminal superhelix composed of 11 TPRs. The thick gray curve follows the right-handed spiral feature of the TPRs. **d**) H2H3 of a second LbcA (magenta cartoon and transparent surface) and H1H4 of a third LbcA (light blue cartoon and transparent surface) insert into the first LbcA spiral, likely mimicking the substrate binding by the first LbcA spiral.

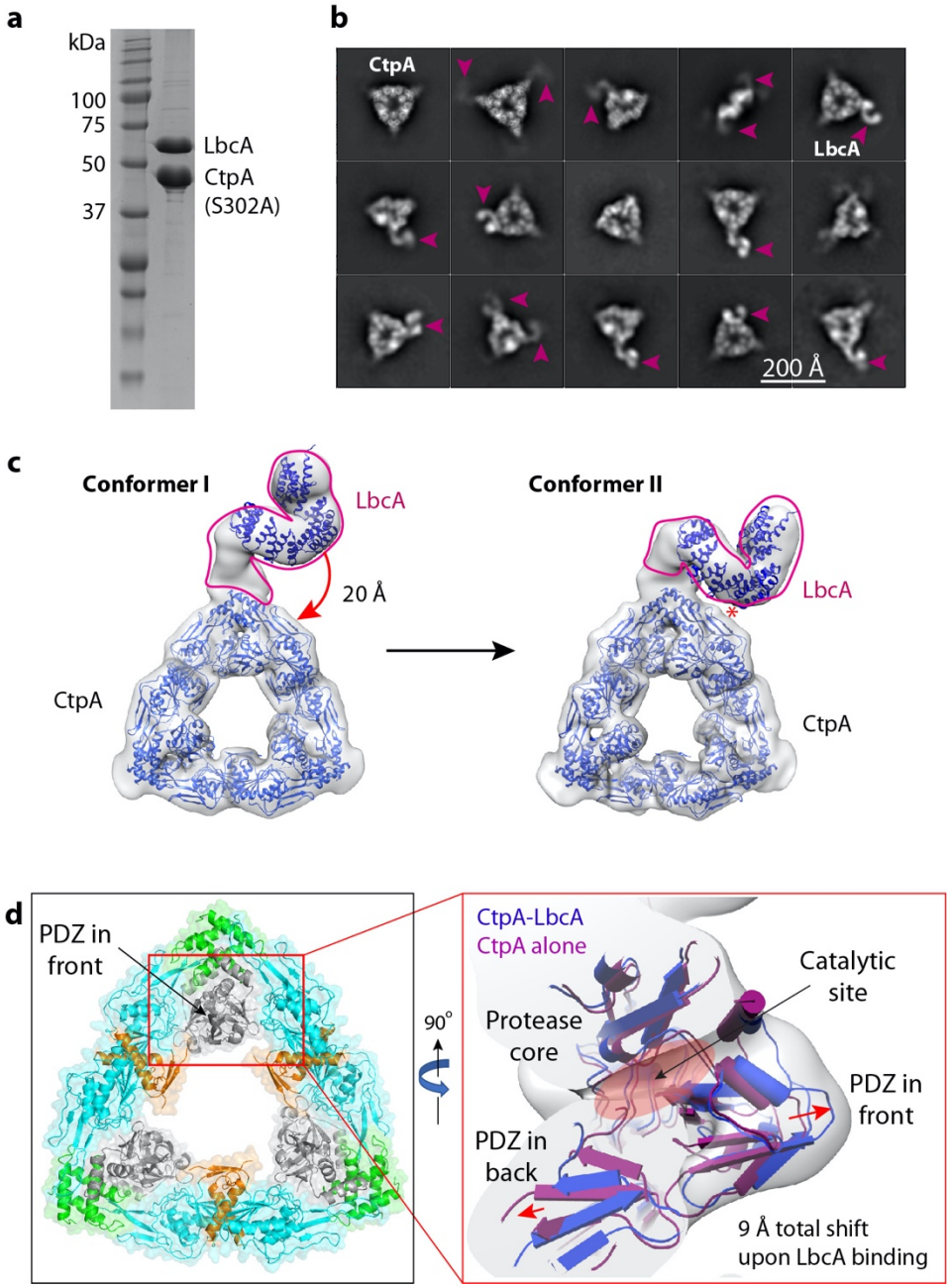

Fig. 5. Cryo-EM 3D maps of the LbcA–CtpA complex. a) Purified LbcA(ΔN47)–CtpA(S302A) complex has an approximate molar ratio of 1:2 LbcA to CtpA, suggesting a 3:6 stoichiometry of the complex. **c**) Cryo-EM 2D averages of LbcA–CtpA shows that up to three LbcA bind to a CtpA hexamer *in vitro*. **d**) Cryo-EM 3D maps of the LbcAΔN31–CtpA(S302A) complex in conformers I and II, rigid-body-docked with the crystal structure of the CtpA hexamer and the LbcA TPR spiral. The red arrow indicates the 20 Å downward movement of the LbcA TPR spiral to engage the CtpA cap region as the complex transitions from conformer I to conformer II. **e**) The PDZ domain shifts upon LbcA binding. Left: Structure of the CtpA hexamer with computationally modeled PDZ domains. Right: Cryo-EM map of CtpA–LbcA as a gray transparent surface. The PDZ domain fitted to the cryo-EM map is blue, and the modeled PDZ position in crystal structure of CtpA hexamer is in purple. The red arrow indicates the PDZ shift outwards by 9 Å upon LbcA binding.

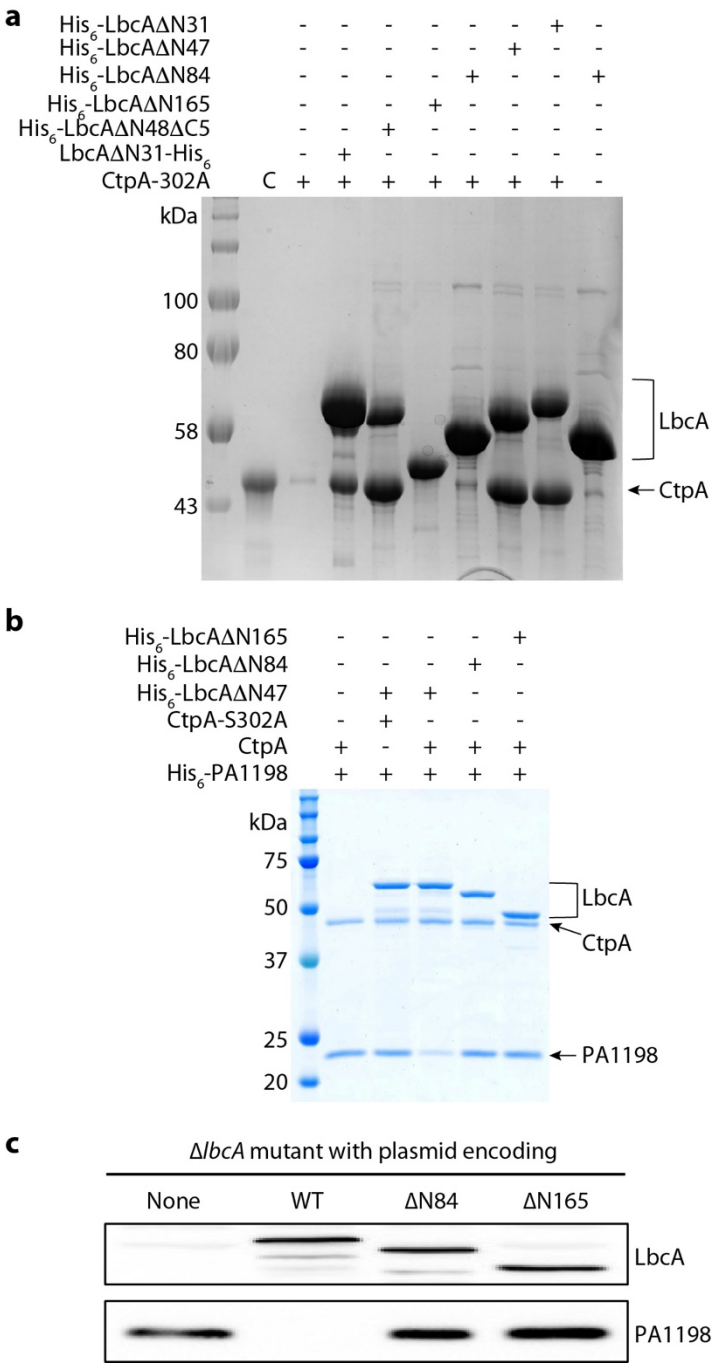

Fig. 6. The LbcA N-terminal extension is essential for the protease activity of CtpA. a) CtpA pull-down assay using various N-terminal and C-terminal deletion mutants of LbcA. Lane 2 is the CtpA input control (C). Lane 3 is the background binding of CtpA to Ni beads. **b**) *In vitro* substrate (PA1198) degradation assay. **c**) Substrate degradation *in vivo*. Plasmids encoding wild-type LbcA (WT), LbcA(ΔN84), or LbcA(ΔN165) were transformed into a *P. aeruginosa* Δ*lbcA* mutant. None = empty plasmid vector control. The LbcA proteins and accumulation of the PA1198 substrate were detected by immunoblot analysis with polyclonal antisera.

581

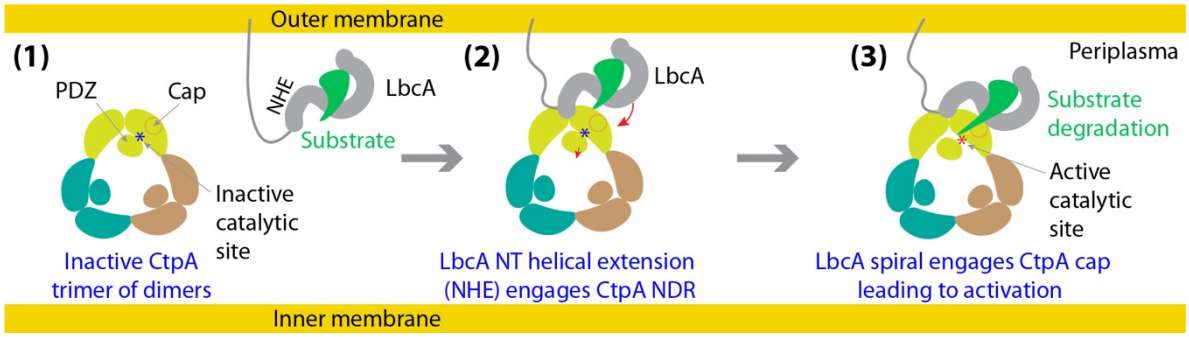

582

583

584 **Fig. 7**. **A proposed mechanism for CtpA activation by LbcA.** Only the three PDZ domains in
585 front of the CtpA hexamer are shown (the three PDZ domain in the back are not). (1) CtpA in
586 the periplasm assembles an inactive hexamer composed of a trimer of dimers. The N-terminus
587 of LbcA is anchored to the outer membrane via the lapidated N-terminal Cys-17 of the mature
588 protein. A 30-residue N-terminal peptide connects the lipid anchor and the ordered region of
589 LbcA, which is composed of a 4-helix N-terminal helical extension (NHE) and the 11-TPR spiral.
590 LbcA could capture the substrate by wrapping around it with its right-handed TPR spiral. (2) The
591 substrate-bound LbcA first engages CtpA by its NHE interfacing with the CtpA N-terminal
592 dimerization region (NDR). (3) LbcA forms a second contract with CtpA: the outer surface of the
593 LbcA spiral moves close to and interacts with the CtpA cap domain. This new contact likely
594 triggers movement of both the cap and the PDZ domains, leading to the formation of the active
595 catalytic pocket and the insertion of the C-terminal peptide of the substrate into the proteolytic
596 site, leading to degradation. See comments in Discussion regarding an alternative model in
597 which CtpA and LbcA are always bound to each other.

598

599 **METHODS**

600 **Protein Expression and Purification of CtpA.** The DNA sequence encompassing from amino
601 acid 38 to the C-terminus of CtpA was subcloned into a pET15b vector between the NdeI and
602 XhoI sites. The resulting plasmid expressed the N-terminal His-tagged CtpA(ΔN37) in the
603 BL21(DE3) strain. For large-scale expression, cells were grown at 37 °C to OD_{600} = 0.6-0.7
604 before being induced with 0.5 mM IPTG. Cells were incubated at 16 °C overnight. After
605 harvesting by centrifugation, cells were lysed by passing through a microfluidizer cell disruptor
606 in 10 mM potassium phosphate, pH 8.0, 10 mM imidazole, and 0.25 M NaCl. The homogenate
607 was clarified by spinning at 27,000 x *g* and the supernatant was applied to a HiTrap-Ni column
608 (GE Healthcare) pre-equilibrated with the lysis buffer. His-tagged proteins were eluted with a
609 10–300 mM imidazole gradient in 10 mM potassium phosphate, pH 8.0, containing 0.25 M
610 NaCl. The fractions containing His-CtpA were collected. The N-terminal His tag was removed
611 using thrombin (0.5 units/mg) by dialyzing against 20 mM Tris, pH 8.0, 150 mM NaCl overnight
612 at 4 °C. The untagged CtpA was further purified with HiTrap-Q in 10 mM Tris, pH 8.0, and a 50–
613 500 mM NaCl gradient and was polished by gel filtration in 10 mM Tris, pH 8.0, and 150 mM
614 NaCl using Superdex 200 prep grade column (16 x 600 mm, GE Healthcare).
615
616 CtpAΔ6 was constructed by deletion of the C-terminal 6 amino acids of CtpA(ΔN37). The
617 expression and purification of CtpAΔ6 and other mutants of CtpA were the same as the
618 CtpA(ΔN37).
619
620 **Protein Expression and Purification of LbcA.** The DNA sequence encompassing from amino
621 acid 49 to the C-terminus of LbcA (LbcA[ΔN48]) was subcloned into the NdeI and HindIII sites of
622 a pET24b vector. For large-scale expression, cells were grown at 37 °C to OD_{600} = 0.5 before
623 being induced with 0.5 mM IPTG. Cells were incubated at 37 °C for another 3 h. The C-terminal
624 6xHis-tagged LbcA was purified with HiTrap-Ni in 10 mM potassium phosphate, pH 8.0, 0.25 M
625 NaCl, and a 10–300 mM imidazole gradient, followed by HiTrap-Q in 10 mM Tris, pH 8.0, and a
626 50–500 mM NaCl gradient. The final polish of LbcA was performed in a Superdex 200 prep-
627 grade column preequilibrated with 10 mM Tris, pH 8.0, and 150 mM NaCl.
628
629 The N-terminal His-tagged LbcA mutants were subcloned into the NdeI and BamHI sites of a
630 pET15b vector. The expression and purification of LbcA mutants were the same as for
631 LbcA(ΔN48).
632

633 **Protein expression and purification of CtpA–LbcA complex.** DNA fragment containing
634 amino acids 32 to the C-terminus of LbcA (LbcA[ΔN31]) was subcloned into the NdeI and BglII
635 sites of a pCDFDuet vector. CtpA(ΔN37, S302A) in pET15b (pET15b_CtpAΔN37) and
636 LbcA(ΔN31) in pCDFDuet (pCDF_LbcAΔN31) were co-expressed in the BL21(DE3) strain. After
637 growing at 37 °C to OD_{600} = 0.7, cells were induced with 1 mM IPTG at 16 °C overnight. The
638 His-tagged CtpA-LbcA complex was first isolated by Hi-Trap Ni with a 10–300 mM imidazole
639 gradient in 10 mM potassium phosphate, pH 8.0, and 0.25 M NaCl. After removing the N-
640 terminal His-tag of CtpA using the thrombin (0.5 units/mg), the CtpA–LbcA complex was purified
641 by Hi-Trap Q in 10 mM Tris, pH 8.0, and a 50–500 mM NaCl gradient, followed by Superose 6
642 Increase (10x300 mm) in 10 mM Tris, pH 8.0, and 150 mM NaCl.
643
644 **Protein crystallization and structural solution.** CtpA(ΔN37) was crystallized at 20 °C by the
645 sitting-drop vapor diffusion method using 0.1 M sodium acetate, pH 4.0, and 0.6 M ammonium
646 dihydrogen phosphate at a concentration of 33 mg/mL. Diffraction data were collected at the
647 Lilly Research Laboratories Collaborative Access Team (LRL-CAT) beamline of the Advanced
648 Photon Source (APS) at Argonne National Laboratory and were processed with Mosflm
649 software. The Se-derived crystals diffracted to 3.3 Å, which is better than the native crystals did,
650 so the Se-derived data were used to solve the CtpA structure. Autosol of Phenix was used to
651 locate Se sites and the resulting map was used to build the initial model. However, the map
652 quality from the SAD method was not good enough to build the CtpA model due to a low
653 anomalous signal (only 4 high-occupancy Se were identified in one asymmetric unit). In
654 combination with molecular replacement, the structure of CtpA(ΔN37) was determined by
655 combining MR-SAD using the core domain of Bs CtpB (PDB ID 4C2C) as the search model.
656 The structure of CtpA(ΔN37, S302A) was solved by PHASER of Phenix using CtpA(ΔN37) as
657 the search model.
658
659 LbcA(ΔN48) was crystallized at 20 °C by the sitting-drop vapor diffusion method using 0.1 M
660 sodium acetate, pH 4.6, and 1.9 M ammonium dihydrogen phosphate at a concentration of 45
661 mg/mL. Diffraction data were collected at the Life Sciences Collaborative Access Team (LS-
662 CAT) beamline of APS and were processed with Mosflm. The best data set was from Se-
663 derived crystal which diffracted to 3.5 Å, so the Se-derived diffraction data were used to solve
664 the LbcA structure. Se sites were determined by the SAD method using Autosol of Phenix. All
665 models of CtpA and LbcA were built in Coot and were refined with Phenix.refine.

666 **Cryo-EM sample preparation and data collection.** Vitrobot Mark IV (FEI, Hillsboro, OR, USA)
667 was used to prepare grids for cryo-EM. A droplet of 3 µL purified CtpA–LbcA complex samples
668 at 0.5 mg/mL were applied to glow-discharged Quantifoil R2/1 300 mesh Au holey carbon grids
669 at 4 °C. Liquid ethane was used as the cryogen and the settings were 100% relative humidity,
670 blotting force 3, and 3 s of blotting time. Cryo-EM data were collected on a FEI Talos Arctica
671 electron microscope equipped with a Gatan K2 Summit direct electron detector. The beam-in-
672 duced motions of the movie stacks were corrected with MotionCor2 and the CTF estimations
673 were done with CTFFIND-4.1. All processing was done in RELION-3 except that the *ab initio*
674 models were generated by Cryosparc-2.8. The flow chart of data processing was outlined in
675 Supplemental Figure 3.

676 ***In vitro* proteolysis assay.** CtpA and LbcA proteins were purified as described above. To purify
677 His_6-PA1198, *E. coli* strain M15 [pREP4] (Qiagen) containing pAJD2948 was grown in 500 mL
678 of LB broth at 37 °C with aeration to an OD_{600} of 0.6-1.0. Protein production was induced by
679 adding 1 mM IPTG and incubation at 37 °C was continued for 3 h, after which cells were
680 harvested by centrifugation. Proteins were purified under native conditions by nickel–
681 nitrilotriacetic acid–agarose affinity chromatography in buffer containing 50 mM NaH_2PO_4 and
682 300 mM NaCl, as recommended by the manufacturer (Qiagen). Protein was eluted in 50 mM
683 NaH_2PO_4, 300 mM NaCl, pH 8 buffer containing 50 mM imidazole. The assays were done
684 similarly to those described previously [22,31]. Reactions were terminated by adding SDS-PAGE
685 sample buffer and incubating at 90 °C for 10 min. Samples were separated by SDS-PAGE and
686 stained with ProtoBlue Safe (National Diagnostics). For the experiments with mutant CtpA
687 proteins, ImageJ analysis was used to determine the densities of the His_6-PA1198 bands. The
688 amount of His_6-PA1198 degraded in each reaction was determined by comparing the His_6-
689 PA1198 band density to that in the reaction with inactive CtpA(S302A). This was done in two
690 independent experiments, with the average values reported.
691
692 ***In vivo* CtpA activity assay**. A DNA fragment encoding wild-type CtpA was generated by
693 amplifying *ctpA* from *P. aeruginosa* PAK chromosomal DNA using one primer that annealed
694 about 30 bp upstream of the *ctpA* start codon and a second reverse primer that annealed
695 immediately downstream of the stop codon. A fragment encoding CtpA(ΔC6) was generated
696 similarly, but with a reverse primer that annealed immediately downstream of codon 430 and
697 incorporated a stop codon immediately after it. Fragments encoding CtpA-L426K L430K or
698 CtpA-L426A L430A were generated by amplifying *ctpA* with reverse primers that incorporated

699 the mutagenic mismatches into codons 426 and 430. A fragment encoding CtpA(S302A) was
700 generated by amplifying *ctpA* from *P. aeruginosa ctpA-S302A* mutant strain AJDP1140 DNA
701 using the same primer pairs used to amplify wild-type *ctpA*. In all cases the fragments were
702 cloned into pHERD26T using EcoRI and XbaI restriction sites added to the fragments by the
703 amplification primers.
704
705 Fragments encoding LbcA(ΔN84) and LbcA(ΔN165) were generated by amplifying one fragment
706 with a forward primer that annealed about 40 bp upstream of the *lbcA* start codon and a reverse
707 primer that annealed at codon 31. A second fragment was amplified with a forward primer that
708 annealed at either codon 85 or codon 166 and a reverse primer that annealed at the *lbcA* stop
709 codon. The forward primer for the second fragments had a 5′ tail complementary to the end of
710 the first fragment (*lbcA* codons 25-31). The first fragment was joined to one of the second
711 fragments by splicing overlap extension PCR [32]. The resulting fragments encoded LbcA with
712 internal deletions that removed codons 32-84 (ΔN84) or codons 32-165 (ΔN165). The retention
713 of codons 1-31 meant that these LbcA proteins retained their signal sequence, followed by 15
714 amino acids corresponding to the N-terminus of mature wild-type LbcA in order to ensure
715 normal signal sequence processing, lipidation, and outer membrane trafficking. A fragment
716 encoding wild-type *lbcA* was generated by amplifying *lbcA* from wild-type *P. aeruginosa*
717 chromosomal DNA using a forward primer that annealed about 40 bp upstream of the start
718 codon and a reverse primer that annealed at the *lbcA* stop codon. In all cases the fragments
719 were cloned into pHERD26T using EcoRI and HindIII restriction sites added to the fragments by
720 the amplification primers.
721
722 The plasmids described above were introduced into *P. aeruginosa* Δ*ctpA* or Δ*lbcA* mutants by
723 electroporation [33]. Saturated cultures of these transformants were diluted into 5 mL of LB broth
724 containing 75 µg/mL tetracycline, in 18-mm diameter test tubes, so that the OD_{600} was 0.05. The
725 cultures were grown on a roller drum at 37 °C for 5 h. Cells were harvested by centrifugation
726 and resuspended in SDS-PAGE sample buffer at equal concentrations based on the culture
727 OD_{600}. Samples were separated by SDS-PAGE and transferred to nitrocellulose by semi-dry
728 electroblotting. Chemiluminescent detection followed incubation with diluted polyclonal antisera
729 against CtpA, LbcA, or PA1198, and then goat anti-rabbit IgG (Sigma) horseradish peroxidase
730 conjugates used at the manufacturer's recommended dilution.

Supplemental Table 1. Strains and plasmids used in this study

Name	Genotype/Features	Reference or Source
***P. aeruginosa* strains**		
PAK	wild-type PAK strain	Ref. 34
AJDP730	PAK Δ*ctpA*	Ref. 22
AJDP1091	PAK Δ*lbcA::aacC1*	Ref. 22
AJDP1140	PAK *ctpA-S302A*	Ref. 22
***E. coli* strain**		
BL21(DE3)	F-$^{-}$ *ompT gal [dcm] [lon] hsdS*$_B$ (r_B^- m_B^-; an *E. coli* B strain) λDE3	Ref. 35
Plasmids		
pCDFDuet-1	Str/Spc^r, CDF ori, *T7p* dual gene expression vector	Novagen
pET15b	Amp^r, pMB1 *ori*, *T7p* expression vector	Novagen
pET24b	Kan^r, pMB1 *ori*, *T7p* expression vector	Novagen
pHERD26T	Tet^r, pMB1 *ori*, *araBp* expression vector	Ref. 36
pQE-30	Amp^r, Col E1 *ori*, *T5p* expression vector	Qiagen
pAJD2948	*T5p-his*$_6$-PA1198 in pQE-30	[a]
pAJD3037	*araBp-ctpA* in pHERD26T	This study
pAJD3038	*araBp-ctpA*Δ*C6* in pHERD26T	This study
pAJD3039	*araBp-ctpA-L426K L430K* in pHERD26T	This study
pAJD3045	*araBp-ctpA-S302A* in pHERD26T	This study
pAJD3063	*araBp-ctpA-L426A L430A* in pHERD26T	This study
pAJD3109	*araBp-lbcA* in pHERD26T	This study
pAJD3110	*araBp-lbcA*Δ*N84* in pHERD26T	This study
pAJD3111	*araBp-lbcA*Δ*N165* in pHERD26T	This study
pET15b_CtpAΔN37	*T7p-his*$_6$*-ctpA*Δ*N37* in pET15b	This study
pET15b_CtpAΔN37ΔC6	*T7p-his*$_6$*-ctpA*Δ*N37*Δ*C6* in pET15b	This study
pET15b_CtpAΔN37_S302A	*T7p-his*$_6$*-ctpA*Δ*N37_S302A* in pET15b	This study

pET15b_CtpAΔN37_L426K/L430K	*T7p-his$_6$-ctpAΔN37_L426K L430K* in pET15b	This study
pET15b_CtpAΔN37_L426A/L430A	*T7p-his$_6$-ctpAΔN37_L426A L430A* in pET15b	This study
pET24b_LbcAΔN48	*T7p-lbcAΔN48-his$_6$* in pET24b	This study
pET15b_LbcAΔN31	*T7p-his$_6$-lbcAΔN31* in pET15b	This study
pET15b_LbcAΔN48	*T7p-his$_6$-lbcAΔN34* in pET15b	This study
pET15b_LbcAΔN84	*T7p-his$_6$-lbcAΔN84* in pET15b	This study
pET15b_LbcAΔN165	*T7p-his$_6$-lbcAΔN165* in pET15b	This study
pET15b_LbcAΔN48ΔC5	*T7p-his$_6$-lbcAΔN48ΔC5* in pET15b	This study
pCDF_LbcAΔN31	*T7p-lbcAΔN31* in pCDFDuet-1	This study

[a] D. Chakraborty and A. J. Darwin, manuscript submitted.

Supplemental Table 2. Crystallographic data collection and refinement statistics

	CtpAΔN37_Se	CtpA(ΔN37, S302A)	LbcAΔN48_Se
Data collection			
Wavelength (Å)	0.97931	1.07803	0.97872
Space group	H3	H3	P 32 2 1
Cell dimensions			
a, *b*, *c* (Å)	187.49, 187.49, 132.01	189.65, 189.65, 131.10	120.70, 120.70, 221.94
α, β, γ (°)	90.00, 90.00, 120.00	90.00, 90.00, 120.00	90.00, 90.00, 120.00
Resolution (Å)	93.75 – 3.30 (3.48 - 3.30)*	94.82 – 3.2 (3.37 – 3.2)*	94.57 – 3.50 (3.69 – 3.50)*
R_{merge} (%)	16.7 (91.2)	8.9 (142)	18.3 (226)
$I / \sigma I$	10.8 (2.9)	15.6 (2.0)	13.2 (2.0)
Total reflections	301572 (44008)	297808 (44906)	536619 (78420)
Completeness (%)	100 (100)	99.6 (99.9)	100 (100)
Redundancy	11.6 (11.4)	10.3 (10.6)	22.1 (22.5)
Refinement			
Resolution (Å)	39.83 – 3.30	43.03 – 3.2	60.39 – 3.50
No. reflections	26026	28849	24277
R_{work} / R_{free}	0.2375 / 0. 2636	0.2422/0.2654	0.2470 / 0.2806
No. of non-hydrogen atoms	3933	3931	8352
Macromolecule	3933	3931	8352
Ligand	0	0	0
Water	0	0	0
B-factors	91.58	126.34	135.73
Macromolecule	91.58	126.34	135.73
Ligand			
Water			
R.m.s. deviations			
Bond lengths (Å)	0.003	0.003	0.003
Bond angles (°)	0.757	0.739	0.608
Ramachandran statistics (%)			
Favored	96.83	97.02	97.89
Allowed	3.17	2.98	2.11
Outliers	0	0	0

*Values in parentheses are for the last (highest) resolution shell.

Supplemental Table 3. Cryo-EM 3D reconstruction of the CtpA−LbcA complex

CtpA-LbcA complex	Conformer I	Conformer II
Data collection and processing		
Microscope	FEI Talos Arctica	
Detector	Gatan K2	
Magnification	36,000	
Voltage (kV)	200	
Electron exposure (e^{-}/Å^2)	54-57	
Defocus range (-μm)	1.2-2.4	
Pixel size (Å)	1.16	
Symmetry	C1	
Initial particle numbers	1,446,732	
Final particle numbers	63,309	136,750
Map resolution (Å) (FSC = 0.143)	8.8	8.1

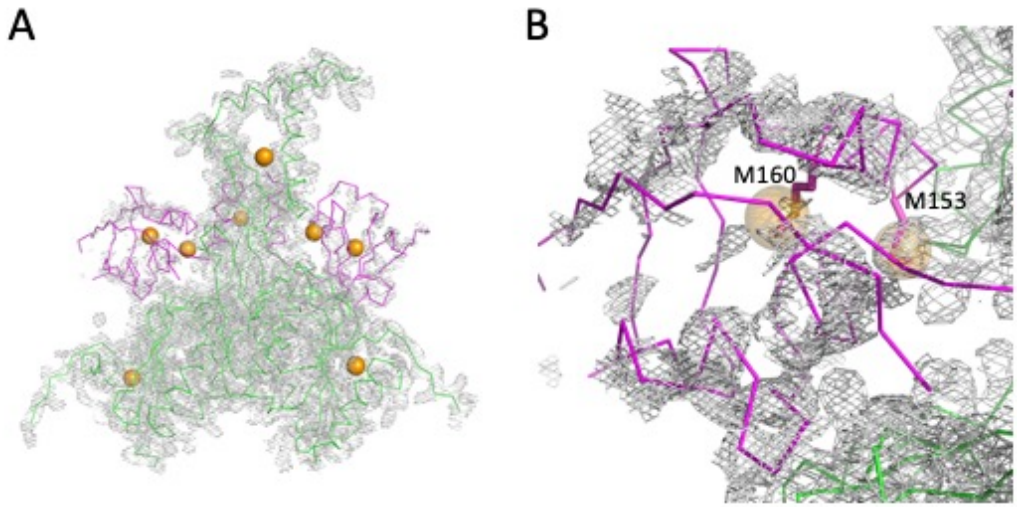

Supplemental Figure 1. Se-Met peaks superimposed with PDZ homolog model. A) The overall electron density map of one asymmetric unit obtained from the Se-derivatized CtpA hexamer crystal. The 2mFo−DFc electron density map is rendered at 1σ threshold and shown as gray meshes. The non-PDZ domains are shown in green and the PDZ domains are show in magenta. The positions of Se are in orange. **B**) Enlarged view of the left PDZ region in (A).

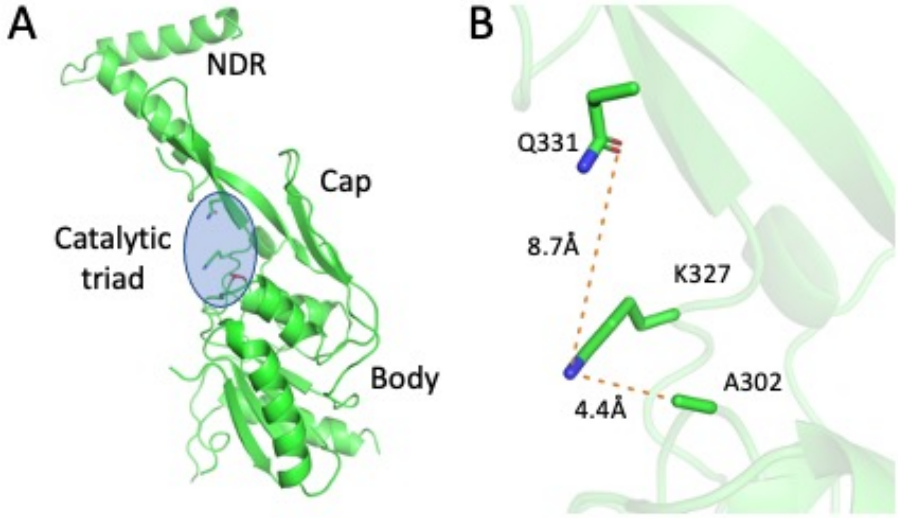

Supplemental Figure 2. Crystal structure of CtpA(S302A) showing only a monomer. A) overall structure of CtpA(S302A) in ribbons, with the catalytic triad residues in sticks and the point mutation S302A in red sticks. **B**) Enlarged view of the catalytic triad in the CtpA(S302A) crystal structure. The structure is also in the inactive configuration.

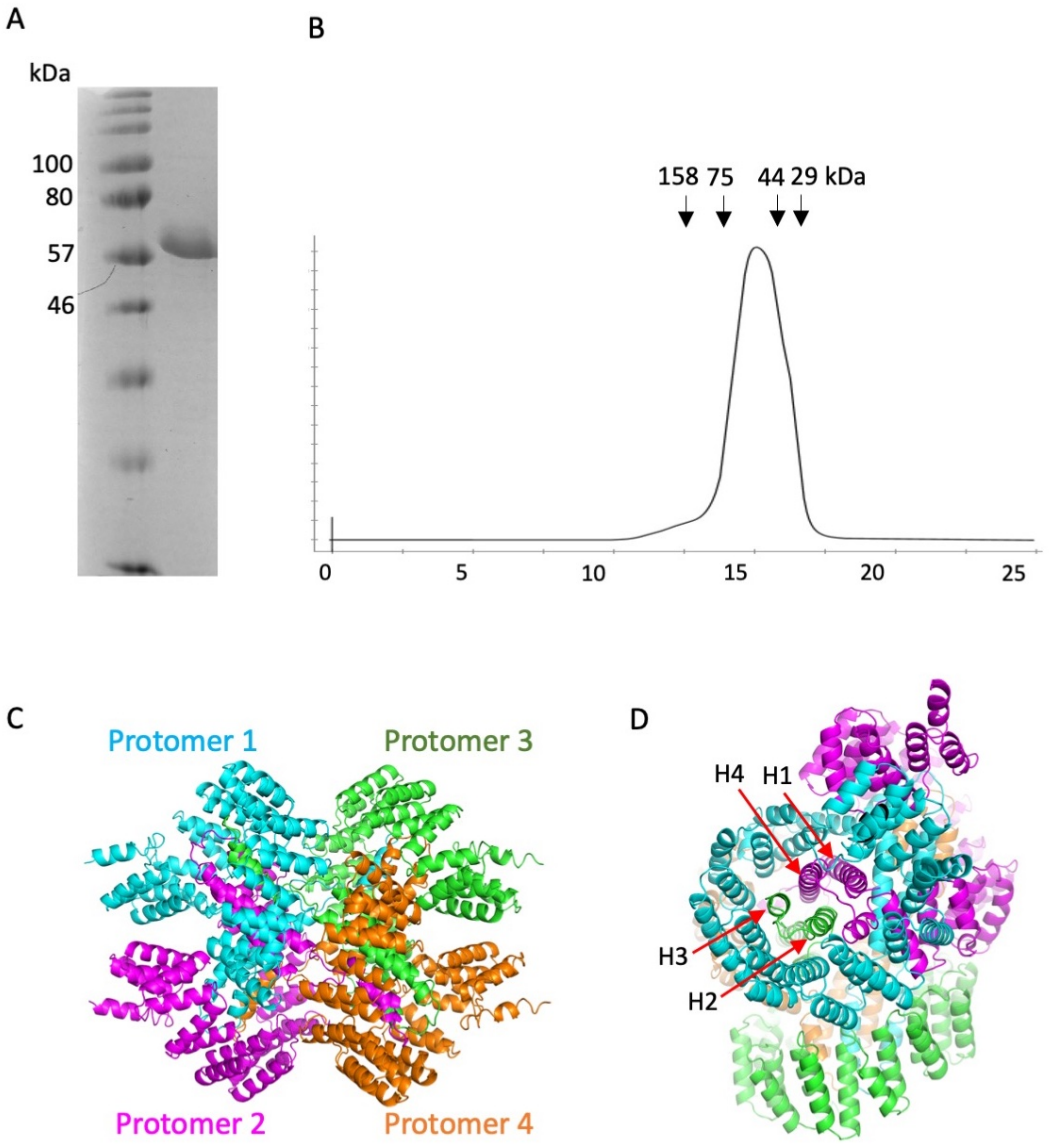

Supplemental Figure 3. LbcA is a monomer in solution but assembles a tetramer in crystal. A) Coomassie blue stained SDS-PAGE gel of the purified of LbcAΔN48. **B**) Superdex-200 elution profile of LbcAΔN48. LbcA was eluted from gel filtration column at a volume corresponding to the monomeric state. **C**) LbcA forms an intertwined tetramer in the crystal lattice. The four protomers are individually colored. **D**) This LbcA tetramer view shows that the helices H1 and H4 of protomer 2 and helices H2 and H3 of protomer 3 form a 4-helix bundle inside the super helical coil of protomer 1 in the crystal lattice.

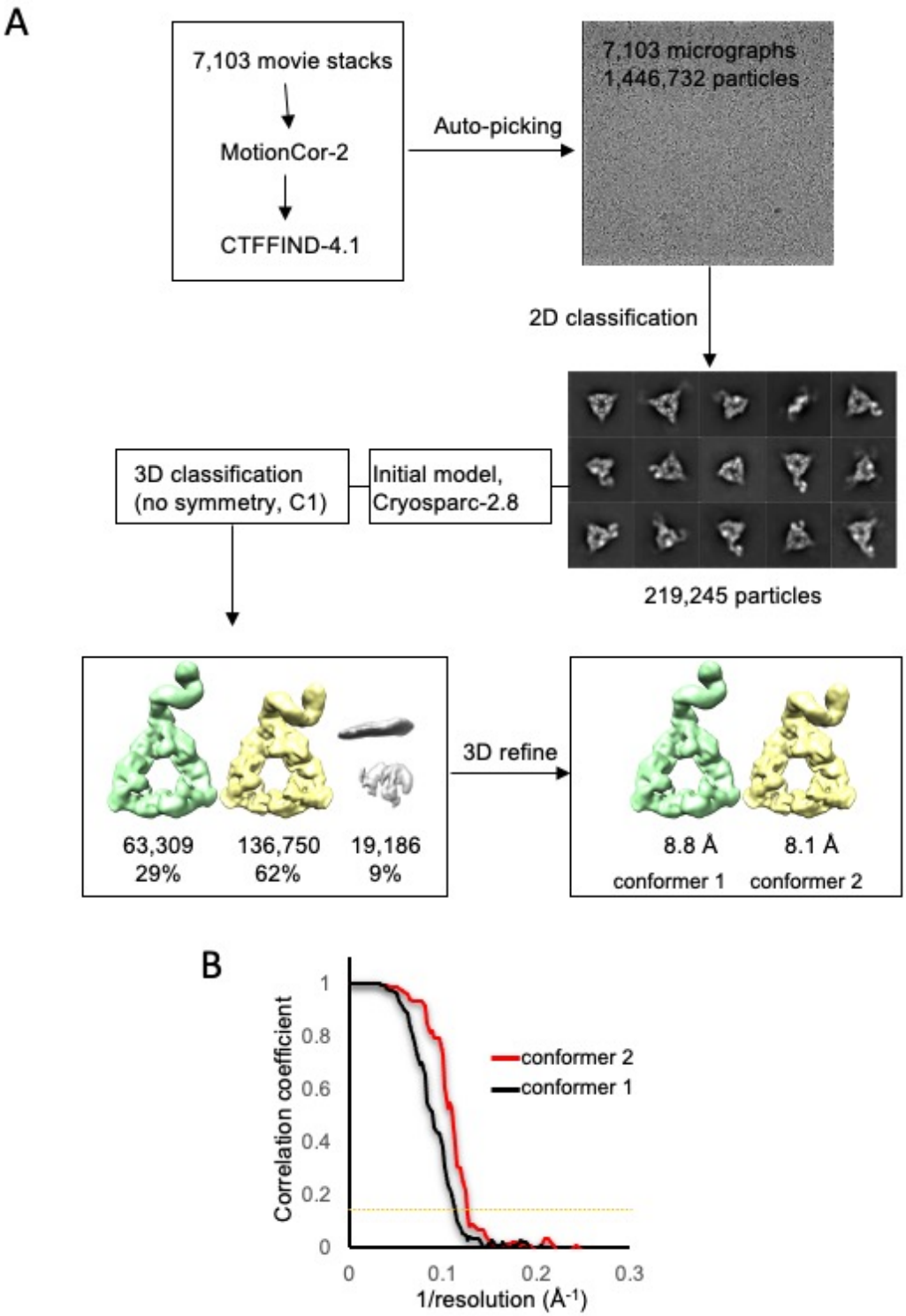

Supplemental Figure 4. Cryo-EM of LbcA−CtpA complex. A) The flow chart of image processing. **B**) Fourier shell correlation curves for conformer I and II. The resolution was determined by the 0.143 threshold.

Supplemental Video 1. CtpA hexamer structure. Rotation of the hexamer, then transition to a monomer to show the domain structure, then transition to morphing between inactive and active computational model (based on CtpB).

Supplemental Video 2: Cryo-EM 3D map of the LbcA−CtpA complex morphing from conformer I to conformer II. Accompanying the LbcA downward movement, the front PDZ domain rotates and moves out of the hexamer plane by 9 Å. These changes likely activate the CtpA protease.